Available online at www.sciencedirect.com
SCIENCE DIRECT®
Journal of Power Sources 145 (2005) 199–205
JOURNAL OF POWER SOURCES
www.elsevier.com/locate/jpowsour

Evaluation of volatile behaviour and the volatilization volume of molten salt in DIR-MCFC by using the image measurement technique

Kimihiko Sugiura [a,*], Makoto Yamauchi [a], Kazumi Tanimoto [b], Yasumasa Yoshitani [a]

[a] *Osaka Prefectural College of Technology, 26-12 Saiwai, Neyagawa, Osaka 572-8572, Japan*
[b] *National Institute of Advanced Industrial Science and Technology– Kansai, 1-8-31 Midorigaoka, Ikeda, Osaka 563-8577, Japan*

Accepted 13 December 2004
Available online 31 May 2005

Abstract

The volatilization of molten salt is one of the factors that control the performance of molten carbonate fuel cells (MCFC). Volatilization of molten salt promotes the cross-leakage and corrosion of metallic components. Moreover, pipe blockage is caused by the solidification of volatile matter. Especially, because reforming catalysts filling the anode channel are polluted by molten salt volatile matter in direct internal reforming molten carbonate fuel cells (DIR-MCFC), volatilizing of the molten salt is a weighty subject. However, neither the behaviour nor the volatilization volume of molten salt volatile matter has been elucidated, because molten salt volatile matter that has strong alkalinity cannot be supplied directly to an analyzer, its volatilization volume is small, and the analytical accuracy is poor. Therefore, an attempt was made to elucidate the behaviour of vaporized alkali hydroxide by using a non-contact image measurement technique. The DIR-MCFC electrolyte is generally $62Li_2CO_3/38K_2CO_3$. Consideration was given to the DIR-MCFC catalyst pollution mechanism as follows. Molten salt volatile matter is KOH generated as water generated in the cell reacts with the electrolyte. The generated KOH returns to K_2CO_3 again in high CO_2 concentration regions, and catalyst pollution is caused by the adherence of the K_2CO_3 to the catalyst. Moreover, the K_2CO_3 particles mutually cohere when the generated water assists bonding and blocks the piping. The present report experimentally evaluates the volatilization volume of KOH, the change from KOH to K_2CO_3, and the particulate growth of K_2CO_3, using the image measurement technique. In measuring the KOH volatilization volume, K_2CO_3 is generated as KOH volatilized by heating it in a crucible in an electric furnace reacts with CO_2, and is then injected into a reaction tube. The amount of K_2CO_3 is measured by measuring the image of the K_2CO_3 particle with a YAG laser and a CCD camera, thereby obtaining the KOH volatilization volume from the calculation of the stoichiometry of the amount of K_2CO_3. In order to study the change from KOH to K_2CO_3, the particulate growth of K_2CO_3 can be monitored by taking a picture of a K_2CO_3 particle generated with KOH and CO_2 for an extended period. As a result, a conglomerate is generated by the mutual adhesion small particles, causing piping blockage.

Keywords: DIR-MCFC; Volatilizing molten hydroxide; Vapour-phase pollution; Image measurement technique

1. Introduction

Direct internal reforming molten carbonate fuel cells (DIR-MCFC) have high-energy efficiency, because the hydrogen generated by the reforming reaction at the anode channel is used for the cell reaction. Moreover, DIR-MCFC can decrease the amount of steam supply by using the water generated in the cell reaction for the reformer reaction. However, in the direct internal reforming molten carbonate fuel cells (DIR-MCFC), deterioration of catalytic activity takes place in the anode channel due to both liquid-phase pollution and vapour-phase pollution [1]. Liquid-phase pollution arises because catalytic activity is deteriorated by molten salts ($62Li_2CO_3/38K_2CO_3$ or $52Li_2CO_3/48Na_2CO_3$) adhering to the catalyst [2], a problem that can be solved by installing a protective barrier in the pollutant pathway [3]. On the other hand, we are convinced that the vapour-phase pollution is due to the deterioration and catalytic activity by KOH (or

* Corresponding author.

0378-7753/$ – see front matter © 2005 Elsevier B.V. All rights reserved.
doi:10.1016/j.jpowsour.2004.12.079

NaOH) adhering to the catalyst [4]. However, reports of the elucidation of the molten salt's volatilization mechanism and the amount of volatilized hydroxide have apparently not been published to date. It is an objective of this study to clarify the vapour-phase pollution mechanism in the DIR-MCFC using the visualization technique by two methods. First, we use visualization of the volatile phenomenon in the cell. Secondly, we use the volatilization volume visualization technique of the volatile matter and the vapour-phase pollution mechanism in ex situ experiments.

2. Visualization of cell reactions in cells

2.1. Experimental apparatus

Fig. 1 shows a schematic diagram of the structure of an anode cell frame with the observation window and the irradiation window. The irradiation window is installed on the front of a cell on the gas inlet side, and the observation window is installed on the side of the cell. The two windows are installed so that the upper parts of the windows are located level with the electrode surface, the window diameter being 7.6 mm. Therefore, though a conventional cell gas channel is 3.0–4.0 mm in depth, the depth of this cell is 10 mm. Moreover, the cell does not use an anode current collector. The anode thickness is half that of a conventional electrode, and the electrolyte-loading ratio is conventional for the three-phase interface so that the reaction field located near the observation window. MCFC components are made by the National Institute of Advanced Industrial Science and Technology– Kansai (AIST).Anode and cathode materials are conventional, and the electrolyte is a (62 + 38) mol% (Li + K)/CO_3 melt. The electrolyte matrix is lithium aluminium oxide, and the electrode area is 16 cm^2. Fig. 2 shows a schematic diagram of the experimental apparatus. The fuel cell temperature is held constant by a heater plate. The anode gas is humidified by passing the humidifier en route to the MCFC. Cell voltage is measured and recorded by a data logger, and the image of the volatile phenomenon is illuminated by a YAG laser light sheet 2 mm thick from an irradiation window into the anode channel. Measurements are made from an observation window with a high spatial-resolution video camera (12 bit). The

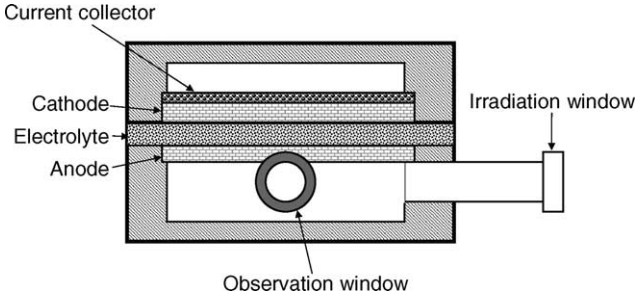

Fig. 1. Schematic diagram of the structure of the anode cell frame with the observation window and the irradiation window.

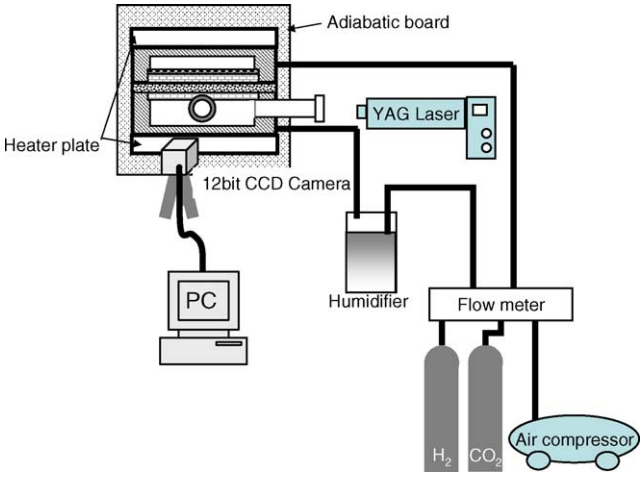

Fig. 2. Schematic diagram of experimental apparatus for visualization in cell.

image picture of 1300 pixel × 1024 pixels spatial-resolution is saved directly into computer memory. The anode standard gas is 70.4H_2/17.6CO_2/12H_2O, and the cathode standard gas is 70air/30CO_2, with each gas utilization being 40%.

2.2. Results and discussions

Fig. 3 shows each measurement image in the anode channel when the current density is changed. Here, the anode is located in the upper part of the measurement image, the gas inlet is located on the right side, and the gas outlet is located on the left. Volatile matter is not observed in an anode channel at OCV. However, volatile matter flows in a ribbon from the inlet side near the electrode toward outlet as the current density increases, and its amount increases. Therefore, it is understood that this volatile matter is a product of the cell reaction. Because the Raman intensity of the volatile matter is too small, the volatile matters could not be identified directly by Raman scattering spectrometry. In this instance, CO_2 and H_2O are product materials of the cell reaction but CO_2 and H_2O, which are gas-phase under cell temperature conditions, cannot be observed. In addition, because the volatile matter is not under the electrode but is present 2–3 mm from the electrode, it requires some time to become an observable solid. Moreover, in experiments that used an electrode of a conventional thickness (0.8 mm), the volatile matter was not observed at all. It is understood that the volatile matter is generated in accordance with the following procedures from the above-mentioned results. (1) The molten salt volatile matter is KOH generated as water generated by the cell reaction reacts with the electrolyte. (2) The generated KOH returns to K_2CO_3 according to Eq. (1) in the region where the concentration of CO_2 rises as a result of the cell reaction. KOH can then be visualized as K_2CO_3 smoke (a solid-phase).

$$2KOH + CO_2 \rightarrow K_2CO_3 + H_2O \quad (1)$$

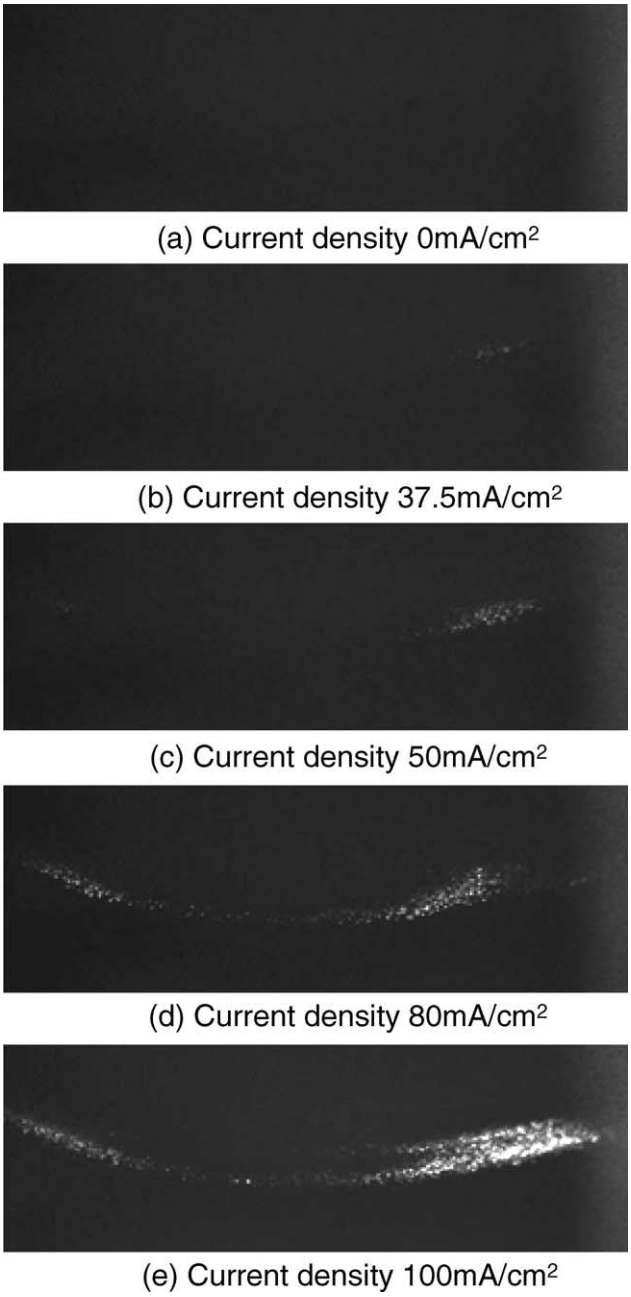

Fig. 3. Measurement image in the anode channel when the current density is changed.

Therefore, catalytic pollution is caused by K_2CO_3 adhering to the catalyst. However, as the conventional anode electrode thickness (0.8 mm) is twice that of this experiment, the dispersion of the volatile matter to the gas channel is rather small for trapping by an electrode without electrolyte.

The electrolyte volatile phenomenon in the cell can be confirmed. However, because the observation conditions are severe in the cell, the experimental conditions cannot be easily changed, and the volume of the volatile matter cannot be measured. Therefore, elucidation was tried using a visualization technique relating to the volatilization volume of the volatile matter and the vapour-phase pollution mechanism in experiments outside the cell (ex situ).

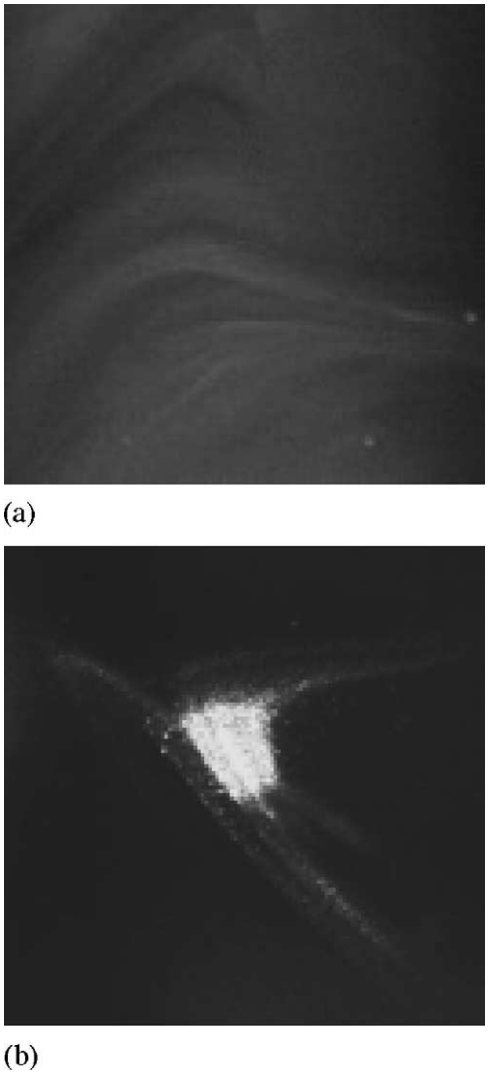

Fig. 4. Measurement image.

3. Elucidating the volatile matter volume by the ex situ experiment

3.1. Experimental apparatus and measuring method

In the visualization experiments in the cell, the volatile matter could be observed by the K_2CO_3 generated as KOH (comprising the volatile matter), which reacted with CO_2 in the cell. Because the image-intensity change of the K_2CO_3 generated corresponds to the concentration change of the K_2CO_3, the concentration of KOH can be measured by measuring the image-intensity change of the generated K_2CO_3. Then the K_2CO_3 generated in the reactor is captured by the CCD video camera, as shown in Fig. 4 (a). Here, Fig. 4 (b) shows the measurement image near the anode elec-

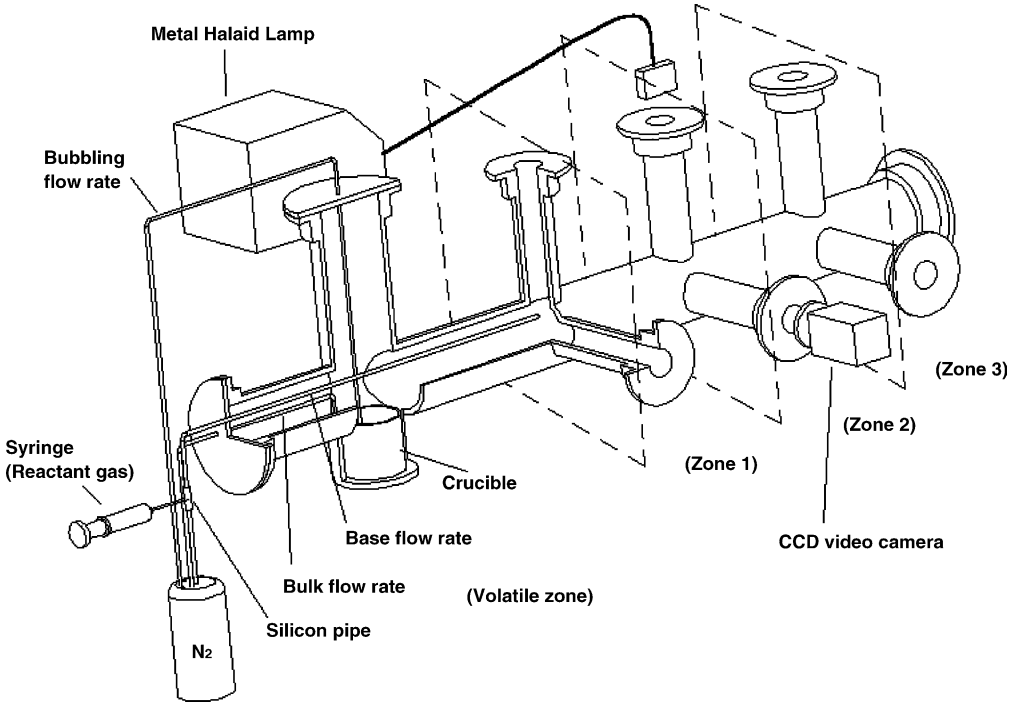

Fig. 5. Schematic diagram of experimental apparatus for visualization without cell.

trode at a current density of 100 mA cm^{-2}. Because the two-measurement images look good, the experiment without the cell can imitate the phenomenon in the cell.

The measurement image Fig. 4 (a) is converted to image-intensity data by an image analysis program. The image-intensity of the generated K_2CO_3 is saturated by increasing the amount of supplied CO_2. As this saturated point corresponds to the amount of volatile KOH, the amount of volatile KOH can be obtained by stoichiometry calculations.

Fig. 5 shows a schematic of the experimental apparatus. The reactor, composed of four sections of a volatile zone and three observation zones, is kept at a preset temperature by using a PID controlled electric furnace. The reactor has an observation window and an irradiation window at each observation zone. A crucible is installed filled with anhydrous potassium hydroxide pellets in the volatile part; and KOH is evaporated by changing its temperature. The reactive part is irradiated from the upper window (irradiation window) provided with two metal halide illumination lights (360 W), and the irradiated image of K_2CO_3 is measured from the front window (observation window) with a 12-bit high spatial-resolution video camera. An image picture of 1300 pixel × 1024 pixel resolution is saved directly into the computer memory every 2 s. The bulk flow of nitrogen is supplied to the volatile zone, and nitrogen is supplied into the crucible to promote the volatilization of KOH. An injection tube, where nitrogen is flowed as carrier gas, is installed from the sidewall of the reactor to the observation window of zone 1. Various amounts of CO_2 are supplied from the injection tube to the reactor in order for the volatized KOH to react into K_2CO_3.

Table 1
Experimental conditions

Bulk flow rate ($cm^3\ min^{-1}$)	1000
Bubbling flow rate ($cm^3\ min^{-1}$)	40
Injection base flow rate ($cm^3\ min^{-1}$)	100
CO_2 injection rate (cm^3)	10, 20, 30, 40, 50, 60 65, 70, 80, 100, 200
Temperature of KOH (°C)	400, 450, 500, 550, 600
Temperature of zone 1–3 (°C)	450

The reactor atmosphere is substituted for N_2 after anhydrous potassium hydroxide pellets in the amount of 50 g are loaded into the crucible. The temperature of the KOH is slowly raised to the melting point (360 °C), and maintained for 3 days to remove water absorbed by the KOH. Moreover, the volatile zone and three observation zones are set to the temperature conditions shown in Table 1.

3.2. Results and discussions

3.2.1. Volatile characteristic of KOH

The amount of generated K_2CO_3 shown in Fig. 4 (a) can be converted to image-intensity by using an image measurement technique. Fig. 6 shows time change lapses relating to the time of image-intensity by changing the amount of the CO_2 supply. Twenty minutes are required to exhaust the K_2CO_3 produced from this reactor under experimental conditions. Then, the time integral value of the image-intensity corresponds to the amount of KOH reacted with supplied CO_2. The mean intensity is defined by dividing the integral value by the experimental time. Fig. 7 shows the relationship between the mean intensity and the amount of supplied

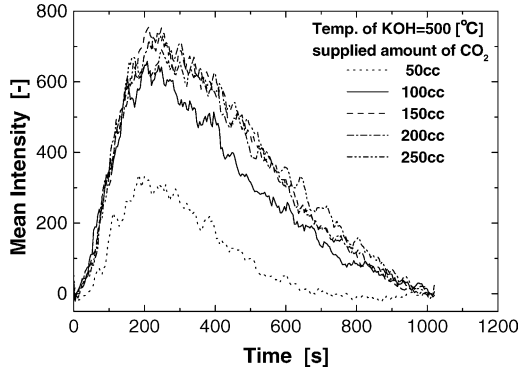

Fig. 6. Change with the lapse of time of image-intensity with changing an amount of the CO_2 supply.

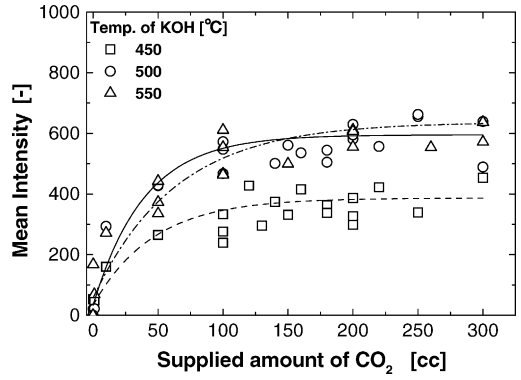

Fig. 7. Relation between the mean intensity and the amount of supplied CO_2.

CO_2. In this figure, the mean intensities obviously have the saturation point for the supplied CO_2. This saturation point means that all of the volatilized KOH has reacted with the CO_2 supplied. Therefore, the amount of volatile KOH at an arbitrary temperature can be estimated from this saturation point. The saturation point set at each temperature is from 100 to 150 cm^3 at 450 °C, and from 150 to 200 cm^3 at 500 °C and from 200 to 250 cm^3 at 550 °C. The volatilized KOH amount is calculated from the stoichiometry of Eq. (1) by using the supplied CO_2 at the saturation point. Fig. 8 shows the

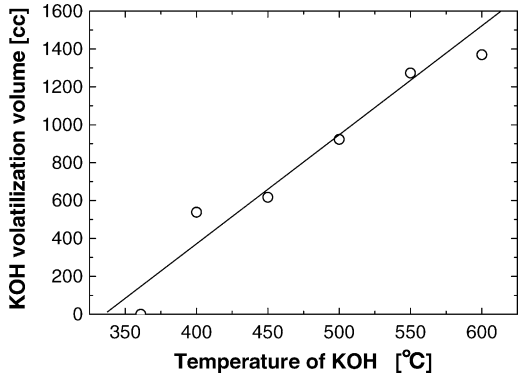

Fig. 8. Volatilized KOH amount at each temperature.

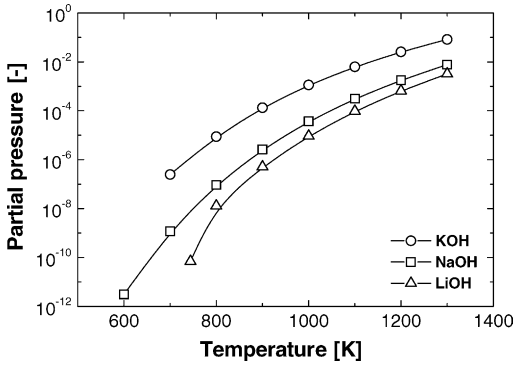

Fig. 9. Partial pressure of each hydroxide.

volatilized KOH amount at each temperature. The volatilized KOH amount is proportional to the temperature.

3.2.2. *Volatile characteristic of Na/LiOH*

Because DIR-MCFC electrolytes are generally $62Li_2CO_3/38K_2CO_3$ or $52Li_2CO_3/48Na_2CO_3$, NaOH and LiOH also have the possibility of existing as volatile matter. Therefore, the difference in the volatile characteristics of NaOH, LiOH and KOH was calculated by using thermodynamics data [5]. Fig. 9 shows the partial pressure of each hydroxide. The amount of each hydroxide is proportional to the temperature, and the amount of volatile NaOH and LiOH is less than that of the KOH. In the DIR-MCFC operating temperature region, the concentration of KOH, NaOH and LiOH is about 10^{-2}%, 10^{-3}% and 10^{-4}%, respectively. The relationship of the volatile characteristics between NaOH, LiOH and KOH are verified by the experiments. Here, as the melting point of NaOH and LiOH is 318 and 471 °C, respectively, the observation zone temperature is set to be higher, at 550 °C, than the melting point of LiOH (471 °C).

Fig. 10 shows the relationship between the mean intensity of Na_2CO_3 and the amount of supplied CO_2. Here, because NaOH hardly volatilizes in the range of temperatures (450–500 °C) used with KOH, Na_2CO_3 particles that had reacted with CO_2 could not be measured. Although the mean intensity of the NaOH is less than that of the KOH,

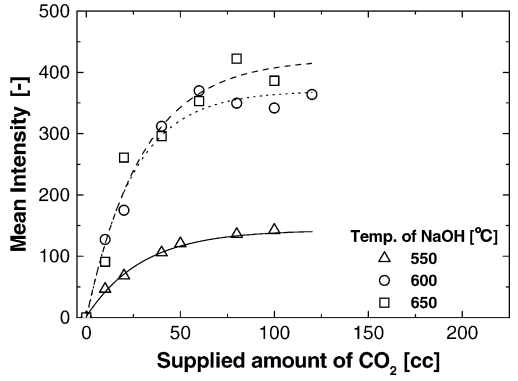

Fig. 10. Relation between the mean intensity of Na_2CO_3 and the amount of supplied CO_2.

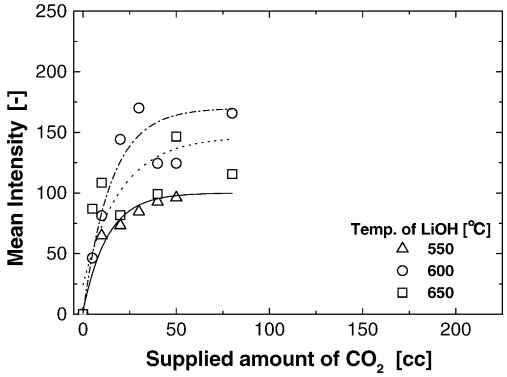

Fig. 11. Relation between the mean intensity of Li_2COs and the amount of supplied CO_2.

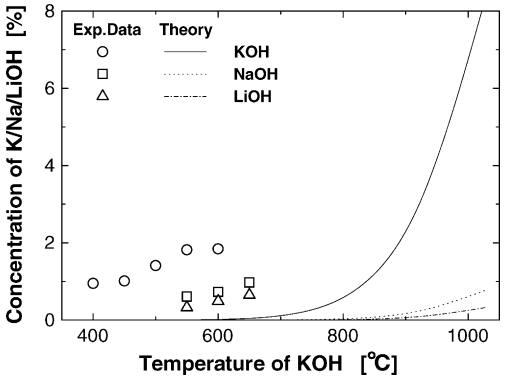

Fig. 12. Comparison between concentrations of volatile K/Na/LiOH and the calculated concentration from thermodynamic data.

the mean intensity obviously has a saturation point for the supplied CO_2 as well as the KOH. Therefore, the amount of volatile NaOH at an arbitrary temperature can be estimated from this saturation point. The saturation point range at each temperature is from 60 to 90 cm^3 at 550 °C, and from 80 to 110 cm^3 at 600 °C and from 100 to 130 cm^3 at 650 °C. As a result, the saturation point of NaOH is smaller than that of KOH.

Fig. 11 shows the relationship between the mean intensity of Li_2CO_3 and the amount of supplied CO_2. The mean intensity of Li_2CO_3 is less than that of Na_2CO_3. The saturation point range at each temperature is from 30 to 50 cm^3 at 550 °C, and from 50 to 70 cm^3 at 600 °C and from 70 to 90 cm^3 at 650 °C. Moreover, the saturation point of LiOH is smaller than that of NaOH. Here, the mean intensity deflection of Li_2CO_3 is larger than that of K_2CO_3 or Na_2CO_3. The reason is that there is a possibility that the dispersion of the corrosion of the alumina tube, etc. exercises an influence because the corrosiveness of the LiOH is stronger than that of other hydroxides. Therefore, it is difficult to suppress the deflection in this image measurement technique, and it limits the application of the image measurement technique.

3.2.3. K/Na/LiOH volatility characteristics

The validity of the volatilization volume of each hydroxide is confirmed from calculated concentrations from thermodynamic data. Fig. 12 shows a comparison between the concentrations of volatile K/Na/LiOH and the calculated concentration from thermodynamic data. Here, the solid line, dotted line and short dashes line refer to the partial pressures of K/Na/LiOH in Fig. 9, respectively. In the operating temperature region (600–650 °C), the thermodynamic data is very low (about 0.01%) while the experimental results are about 1–2%. The difference between the two values is considerably great. If the thermodynamic data is correct, the DIR-MCFC does not have any problem such as catalyst pollution and channel blockage of a heat exchanger. However, although the volatility of $62Li_2CO_3/38K_2CO_3$ molten salt in DIR-MCFC is worse than that of KOH, these problems did occur in the DIR-MCFC, and volatile matter was confirmed, and was increased by increasing the current density near the anode. Therefore, we can understand that the water produced in the cell reaction promotes volatilizing of the molten salt. Moreover, these results suggest that the amount of the vapour-phase pollution in DIR-MCFC is more than predicted in the thermodynamic data, and $Li/NaCO_3$ is better than Li/KCO_3 as an electrolyte.

4. Conclusion

The objective of this study is to evaluate the volatile behaviour and the volatilization volume of molten salt in DIR-MCFC by using the image measurement technique. The results obtained in this study are summarized as follows.

(1) The volatile phenomenon in the cell can be visualized using the image measurement technique.
(2) Though the volatile matter is not observed in the anode-channel at OCV, it has a ribbon-like flow near the electrode when current flows and its amount increases with current density.
(3) The amount of the volatile KOH, calculated from the saturation region of mean intensity, is larger than that predicted form thermodynamic data.
(4) This study suggests that the amount of the vapour-phase pollution in DIR-MCFC is greater than that predicted form thermodynamic data.
(5) Volatility decreases in the order of KOH, NaOH, and LiOH.
(6) It is suggested the mechanism of vapour-phase pollution of DIR-MCFC is as follows: (i) molten salt volatile matter is KOH generated as the water generated by the cell reaction reacts with the electrolyte, (ii) the KOH generated returns to K_2CO_3 again in the region where the CO_2 concentration rises as a result of the cell reaction and (iii) the catalyst pollution is caused by this K_2CO_3′s adhering to the catalyst.

Acknowledgment

This work was supported by Grant-in-Aid for Scientific Research from the Ministry of Education, Science and Culture of Japan (Basic research-C: 15560193).

References

[1] C. Hirai, M. Matsumura, T. Tanaka, Studies on reforming catalyst for internal reforming molten carbonate fuel cell, Abstract Book of Denchi-Touron-kai in Japan (1988) 79–80.

[2] K. Sugiura, K. Ohtake, Deterioration of a catalyst's activity by liquid-phase MC poisoning in DIR-MCFC, J. Chem. Eng. Jpn. 21 (No. 6) (1995) 1170–1178.

[3] Y. Miyake, N. Nakanishi, T. Nakajima, Y. Itoh, T. Saitoh, A. Saiai, H. Yanaru, A study on degradation phenomena of reforming catalyst in DIR-MCFC, J. Chem. Eng. Jpn. 21 (No. 6) (1995) 1104–1109.

[4] K. Sugiura, I. Naruse, K. Ohtake, Deterioration of a catalyst's activity in direct internal reforming-molten carbonate fuel cells (effect of adsorption of vapour-phase molten carbonate), J. Jpn. Soc. Mech. Eng. 65 (No. 629) (1999) 330–336 (Series B).

[5] JANAF Thermochemical Tables, third ed., vol. 14 (1985), pp. 606–608, 628, 1219–1222, 1273–1275.